THE JOURNAL OF PHYSICAL CHEMISTRY C

pubs.acs.org/JPCC Article

Low-Energy CO Scattering at the Gas−Liquid Interface: Experimental/Theoretical Evidence for a Novel Subthermal Impulsive Scattering (STIS) Channel

Timothy A. Livingston Large and David J. Nesbitt*

Cite This: https://dx.doi.org/10.1021/acs.jpcc.0c06400 Read Online

ACCESS | Metrics & More | Article Recommendations

ABSTRACT: Molecular beams of supersonically cooled ($T_{rot} \approx$ 10 K) carbon monoxide (CO) have been scattered from three low-vapor-pressure liquids (PFPE, squalane, and glycerol) over a range of surface temperatures (253−303 K), with the final rovibrational distributions probed by shot-noise-limited direct IR laser absorption methods. Specifically, the present work focuses on quantum-state-resolved scattering at low incident energies ($E_{inc} \leq$ 1.0 kcal/mol), which would normally be expected to yield pure trapping desorption (TD) dynamics with CO in complete thermal equilibrium with the liquid ($T_{rot} \approx T_S$). By way of contrast, the nascently scattered CO(J) exhibits both rotational (T_{rot}) and Doppler translational (T_{Dopp}) distributions distinctly colder than T_S, a phenomenon which is systematically reiterated over a wide range of liquid temperatures. To help identify the relevant collision physics responsible for this surprising subthermal behavior in CO, high-level *ab initio* potentials and detailed molecular dynamics simulations are explored for a series of projectiles (CO, DCl, and CO_2) with varying strengths of interaction with the liquid. At low incident energies, each of the more strongly interacting DCl and CO_2 projectiles is found to thermalize with the liquid interface ($T_{rot} \approx T_S$), while CO is predicted to emerge colder than the surface ($T_{rot} < T_S$) and in remarkably quantitative agreement with experiment. Statistical analysis of the trajectories identifies that CO spends substantially less time and penetrates less deeply into the surface compared to DCl/CO_2 projectiles due to a combination of a shallow van der Waals well and a steep repulsive wall. The simulations reveal that low-energy CO does not undergo conventional trapping desorption (TD) at the gas−liquid interface but instead exhibits incomplete warming from its jet-cooled value ($T_{rot} \approx$ 10 K) via an unexpected *subthermal impulsive scattering* (STIS) pathway. The data suggest that non-equilibrium IS dynamics at low energies may play a crucial role in inelastic energy transfer and thermal accommodation at the gas−liquid interface for weakly interacting collision systems.

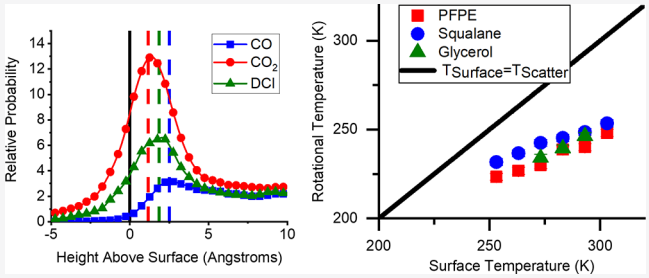

I. INTRODUCTION

Ever since the earliest experimental attempts to probe fundamental scattering at the gas−liquid interface, compelling evidence has been reported for two physically distinct pathways.[1−4] The first is the thermal desorption pathway (TD), whereby the incident molecular projectile traps transiently on the liquid surface and undergoes multiple collisional interactions, which causes it to lose all memory of the incident collision conditions (e.g., speed, direction, quantum state), and desorb in perfect equilibrium with the liquid temperature (T_S). This TD pathway has been presumed to dominate at collision energies comparable to the surface temperature ($E_{inc} \approx kT_S$), as confirmed by multiple energy-dependent studies of the final external (i.e., translational) and internal (i.e., rovibrational) quantum-state distributions.[5,6] To help minimize further potential confusion in literature, we note that such TD dynamics (i.e., "complete loss of incident quantum state memory") is consistent with but does not strictly require the final distribution to be in perfect equilibrium with T_S. As one specific example, non-equilibrium distributions are in fact rigorously predicted by detailed balance considerations if there is some potential energy barrier (e.g., in a projectile-surface displacement or angle) serving as a transition-state bottleneck along the desorption coordinate. This is known to be the case, for example, for H_2 molecules scattering from Ni, Pt, and Fe for which a potential barrier in the adsorption coordinate results in high p_z momentum distributions and narrower than cos(θ) angular distributions in the corresponding desorption dynamics.[7] This behavior has also been seen in a multitude of systems[8] such as the oxidation of CO on Rh(111), which has an exit channel barrier for the

Received: July 13, 2020
Revised: November 24, 2020

product (CO_2) leaving the surface.[9] Evidence for such transition-state barrier complications in quantum-state-resolved scattering studies at the gas−liquid interface has not been reported to date. However, given the rapid progress in this field, we feel it is likely only a matter of time, apparatus sophistication, and experimental sensitivity before such evidence will emerge.

As the familiar counterpart to TD, a second dynamical pathway emerges as a function of increasing collision energy-dubbed impulsive scattering (IS), whereby the molecules retain a partial memory of the incident collision conditions. One of the earliest papers to identify and label this channel was published by Hurst et al.[10] As noted by Hase and co-workers, this molecular memory is not an experimental observable, and thus, such a "catch-all" pathway has no *a priori* rigorous definition.[11] For example, were the IS dynamical pathway to result in distributions that coincidentally matched those of pure TD scattering, these would be indistinguishable from (and by definition subsumed into) the TD pathway. Experimentally, however, distinguishable IS and TD pathways are routinely observed in numerous quantum state-resolved and time-of-flight (TOF) gas−liquid scattering studies.[1,5,12−15] Particularly under glancing incident scattering conditions, such IS deviations from pure $\cos(\theta)$ TD thermalization dynamics have been empirically well described by an additive, near-specular component with translational distributions often hotter than the surface (although not necessarily Boltzmann) and with an average energy content scaling with the incident collision energy. A schematic cartoon of these two pathways is illustrated in Figure 1, which portrays these two limiting pathways of (i) pure $\cos(\theta)$ and (ii) quasi-specular angular distributions for the TD and IS pathways, respectively.

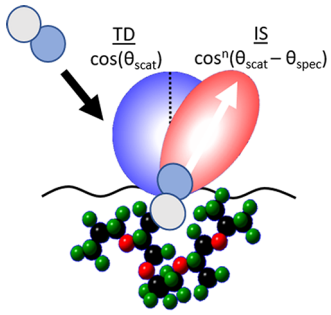

Figure 1. Schematic of the TD/IS gas−liquid scattering paradigm.

Although no predictive theory currently exists that successfully recapitulates all observed gas−liquid scattering behavior, there have been several heuristic models that capture much of the essential physics. For example, a pioneering work by Tully and co-workers on the IS pathway for gas single-crystal scattering has been based on an inertial ("hard cube") description of the local surface response.[16] Minton and co-workers extended these ideas into a simple but elegant kinematic collision model that succeeds in reproducing in-plane angular distributions for IS scattering based on the effective mass of such a cube.[17] One recurring conundrum, particularly evident for projectiles with internal (e.g., rotational/vibrational) degrees of freedom, is that the IS scattering distributions have often appeared hot but Boltzmann, i.e., well described by a hyperthermal IS "temperature," despite the absence of any reason why such a pathway should appear thermal. Fresh insights into this long-standing puzzle have been provided by recent work ("lever arm model"), which reveals that averaging over the collision dynamics (e.g., capillary wave spatial fluctuations of the gas−liquid interface) can convert highly structured impulsive rainbow-like scattering distributions into a remarkably thermal-like distribution without invoking any equilibration.[18] However, no model has yet been forwarded that can predict these effective IS temperatures *a priori* and/or branching ratios (α) into IS/TD channels.

Thermal desorption, conceptually the simpler of the two IS/TD pathways, is thought to be the more universal process in gas−liquid scattering.[19] For gas−liquid systems studied with internal quantum-state resolution, the standard paradigm has been that atoms/molecules undergo complete TD scattering behavior ($\alpha \approx 1$) at low collision energies ($E_{inc} \sim kT_S$) with finite branching ratios ($\alpha < 1$) into IS versus TD pathways appearing only at hyperthermal energies.[5] As one of many systems, CO_2 gas−liquid scattering has been studied with full rovibrational quantum state and Doppler velocity resolution,[1] which for multiple liquids, surface temperatures, and incident angles demonstrate pure TD ($\alpha \approx 1$) at low collision energies and mixed TD/IS behavior ($\alpha < 1$) only at higher energies.[5,20] Indeed, it was largely based on this early work that such "dual temperature" models ($T_{TD} \approx T_S$, with T_{IS} treated as an empirical parameter) were originally postulated for molecular systems probed with both internal and external degrees of freedom.

The most robust empirical support for a dual temperature TD/IS pathway has been found in scattering studies with HCl/DCl. From time of flight studies by Nathanson and co-workers in the forward scattering direction, it was established that HCl/DCl undergoes complete thermalization and $\cos(\theta)$ desorption from several liquid surfaces.[21−23] This was subsequently reinvestigated with both IR direct absorption and REMPI/VMI measurements, which confirmed that HCl/DCl at low energies equilibrates and undergoes thermal desorption in both external (translational) and internal (rotational) degrees of freedom ($T_{trans} \approx T_{rot} \approx T_S$).[18,24] The REMPI/VMI studies at higher collision energies took this one step farther and showed that, due to extreme glancing incident angles (75°), J state populations from both TD and IS pathways could be extracted by separate analysis of the backward and forward velocity components, respectively. This permitted a novel and completely independent test of the dual-temperature TD/IS paradigm, demonstrating that the IS distributions still appear Boltzmann-like but with $T_{IS} >> T_{TD}$ and yet TD distributions with $T_{TD} \approx T_S$. Evidence for such thermal equilibration of the TD fraction to the surface temperature T_S has been seen in many other gas−liquid scattering experiments, for example, McKendrick, Minton, and coworkers report this for OH[25] + hydrocarbon surfaces and O_2 + squalane.[17] The one notable exception for this paradigm has been NO,[26−28] which, at low collision energies, has been reported to scatter with rotational temperatures colder than the liquid surface. Specifically, T_{rot} was found to increase monotonically with surface temperature but with an incremental slope (dT_{rot}/dT_S) less than unity.[26−28] Subthermal behavior at low collision energies has been also seen in NO scattering from single-crystal metals and attributed to a combination of dynamical barriers and further rationalized by the complicated open-shell rovibronic structure of NO.[29−31] A work by Polanyi et al., however, has shown that even the related closed-shell CO exhibits a lack of equilibration with

https://dx.doi.org/10.1021/acs.jpcc.0c06400
J. Phys. Chem. C XXXX, XXX, XXX−XXX

respect to T_S in scattering from single-crystal LiF (001).[32] Based on these results, one might therefore anticipate similar anomalies in low-energy CO scattering of supersonic beams from gas−liquid interfaces.

In this paper, we explore the concept of thermal desorption in scattering experiments through both low-energy quantum-state-resolved scattering and molecular dynamics studies. The paper is organized as follows. First, we describe the experimental methodology in section II, followed in section III by low-energy scattering results as a function of liquid-type (perfluorinated polyethers (PFPE), nonpolar hydrocarbons, and polar glycerol) and liquid surface temperature (T_S = 253−303 K), for each of which the final quantum-state distributions are notably cooler than T_S. To help interpret these experimental results, we present molecular dynamics calculations in section IV.A−D, based on atom−atom intermolecular potentials for CO, DCl, and CO_2 colliding with a fluorinated self-assembled monolayer surface (FSAMs), which prove to be in remarkably quantitative agreement with the experiment. We exploit these simulations to examine projectile-dependent interaction times at the gas−liquid interface and extend the MD results over a larger temperature footprint (T_S = 50−450 K), to elucidate the T_S-dependence on the collision dynamics. Finally, a discussion of possible reasons for this "sub-thermal impulsive scattering" (STIS) behavior for CO versus HCl, CO_2 is presented in section V, with conclusions summarized in section VI.

II. EXPERIMENTAL SECTION

A detailed overview of the experimental apparatus has been presented elsewhere, and thus, only essential details and modifications for the current studies need be described.[5,18,33] This experiment consists of three key components: (i) a temperature-stabilized liquid scattering target, (ii) a supersonic molecular beam, and (iii) a narrow linewidth, shot-noise-limited infrared absorption spectrometer. The temperature-stabilized scattering target is a modified version of the "lazy Susan" apparatus described in previous studies.[33] The liquid surface is prepared according to the method of Lednovich and Fenn,[19] using a rotating (∼0.2 Hz) wheel (12.7 cm diameter) half-submerged in the liquid reservoir and scraped with a stationary razor blade to present a thin (∼500 um), freshly prepared gas−liquid surface to the impinging molecular beam. To facilitate the temperature-dependent studies, we have replaced the Teflon liquid reservoir with a copper reservoir and the glass wheel by a bead-blasted stainless steel wheel to promote adhesion, with the liquid interfacial temperature-stabilized by a two-stage thermoelectric cooling system. A recirculating ethanol chiller (Lauda K-4/R) is used to regulate the temperature of a cold plate in the vacuum chamber from $-T_S \approx 20$ to 30C. (Companies are named in the interest of completeness and not intended as commercial product support.) One side of this plate is attached to the lazy Susan apparatus and the other side to a thermoelectric cooler (TEC) attached to the fluid-filled copper reservoir. A thermistor attached directly to the copper vessel permits the TEC to servo-loop stabilize the reservoir to a primary target T_{res}, with the wheel temperature maintained within 1 °C of the desired setpoint. This reduces temperature gradients across all elements in thermal contact with the scattering fluid, which strengthens confidence that the liquid wheel surface is maintained at a well-determined temperature limited by thermistor uncertainty (±0.5 K).

These studies involve three different classes of liquids that sample different scattering dynamical regimes: (1) perfluorinated polyether, (PFPE, Krytox 1506, F-$[CF(CF_3)-CF_2O]_{14(avg)}$-$CF_2CF_3$), as a rough but chemically inert liquid surface, (2) squalane (2,6,10,15,19,23-hexamethyltetracosane, $C_{30}H_{62}$), as a strongly hydrophobic surface, and (3) glycerol (1,2,3-propanetriol, $C_3H_8O_3$), as a strongly hydrophilic surface due to multiple protruding OH groups.[34] Each liquid is degassed under an ∼1 mTorr vacuum (1 Torr = 133 Pascal) at room temperature for several hours to remove dissolved gases (H_2O, O_2, N_2, CO_2), or at slightly elevated temperatures (∼350 K) for the glycerol liquid samples to allow for more complete degassing within a reasonable time frame.

A low collision energy molecular beam is generated through a Proch and Trickl[35] style pinhole valve, with 5% CO in argon expanded through a 500 um diameter pinhole at 100 Torr backing pressure. These low stagnation pressures are chosen intentionally to maximize CO signals while minimizing Ar−CO clustering in the incident beam. This 5% beam composition leads to an on-axis mean velocity of 550(30) m/s measured with a time of flight microphone setup[36] yielding an average beam energy of E_{inc} = 1.0(1) kcal/mol. The resulting molecular beam is collimated with a 3 mm diameter skimmer (Beam Dynamics), 2.25 cm from the pinhole orifice for a HWHM beam divergence of $\theta \approx 3.82°$, with rotational temperatures of ∼10(2) K measured along the beam expansion axis using the infrared spectrometer described below. The pulse valve is aligned so the center of the molecular beam strikes the surface at $\theta_{inc} \approx -65°$ away from normal incidence, with this highly glancing incident-angle geometry chosen to maximize positively scattered CO absorption signals ($\theta > 0$) while minimizing CO(low J) contamination from the incident beam. Signals are collected in an angular wedge from $\theta \approx -40$ to 75°, with the peak collection efficiency around the specular direction ($\theta_{spec} \approx +65°$) and 2/3 of the collected molecules coming from greater than 45°. For rotational states $J \geq 5$ ($E_{rot} \geq 60$ cm^{-1}), the CO background ($A_{background} \sim 3 \times 10^{-5}$) due to incident beam contamination is an order of magnitude smaller than typical peak absorbance signals ($A > 4 \times 10^{-4}$) due to scattering.

The scattered populations are measured with a tunable laser direct absorption spectrometer operating near the quantum shot-noise limit. This spectrometer consists of (i) a narrow linewidth external cavity quantum cascade laser (ECQCL, Daylight Solutions, 21047-MHF-013-D0724),[37] (ii) frequency calibration/diagnostics, and (iii) an *in vacuo* multipass cell with quantum shot-noise-limited balanced detection. The ECQCL provides CW output greater than 250 mW over a frequency range of 1960−2200 cm^{-1} with an optical linewidth $\Delta\nu < 10$ MHz in the experimental detection bandwidth (10 KHz). The laser frequency is calibrated with the combination of a fixed Fabry Perot etalon (FSR = 249.566(33) MHz) and a 5 cm gas transmission cell (500 mTorr of CO), which allows for both absolute (∼5 MHz) and relative (∼100 ppm) frequency diagnostics. The IR laser beam makes 16 passes through the scattering region in the vacuum chamber, with the light detected on two balanced InSb photodiodes (one before/after the multipass cell) in a fast servo subtraction circuit, removing common-mode technical noise down to the quantum shot-noise limit. The net absorption sensitivity of the system is approximately 7×10^{-8} per Hz$^{1/2}$, which translates into a CO number density detection sensitivity of order a 3×10^8 #/cm^3/quantum state.

https://dx.doi.org/10.1021/acs.jpcc.0c06400
J. Phys. Chem. C XXXX, XXX, XXX−XXX

III. EXPERIMENTAL RESULTS AND ANALYSIS

CO scattering from a series of liquids has been performed as a function of liquid surface temperature (T_S) to characterize the scattering pathways under low-energy collision conditions (E_{inc} = 1.0(1) kcal/mol). The absorption signals reflect column integrated densities ($\rho_{v,J}$), which cannot be deconvolved into fluxes without prior knowledge of the coupled angular/speed scattering distribution ($f(v,\theta,\phi)$).[5,18] We can, however, express the experimental absorbance at a given Doppler detuning ($\nu_{Doppler}$) as the double integral

$$A(v, J, \nu_{Doppler}) = \int d\nu' \int dl[\rho_{v,J}(l, \nu')\sigma(\nu_{Doppler} - \nu')] \quad (1)$$

where $\rho_{v,J}(l,\nu')$ is the quantum-state-resolved density of absorbers at position l along the absorption path, and $\sigma(\nu_{Doppler}\text{-}\nu')$ is the homogeneous absorption cross section per molecule ($cm^2/\#$). Since $\sigma(\nu_{Doppler}\text{-}\nu')$ is much narrower than the Doppler widths, the integral over ν' can be performed to yield

$$A(v, J, \nu_{Doppler}) = S_{0J',v',J,v} \int dl\, \rho_{v,J}(l, \nu_{Doppler}) = S_{0J',v',J,v}\, P_{scatter}\, \rho_{CID} \quad (2)$$

where S_0 is the integrated absorption cross section ($cm^2cm^{-1}/\#$) for the $v' \leftarrow v$, $J' \leftarrow J$ rovibrational transition, ρ_{CID} is the column integrated density ($\#/cm^2$), and $P_{scatter}$ is the total probability of scattering into the v, J quantum state. The experimental absorption profiles are therefore a function of three variables, J, v, and $v_{Doppler}$, where $v_{Doppler}$ is the velocity component along the laser beam axis and probed by Doppler tuning over the rovibrational transition. The laser beam is perpendicular to both the liquid surface normal and molecular beam. The Doppler widths measure the velocity components perpendicular to the scattering plane created by the surface and molecular beam, which will be referred to as the out-of-plane velocity distribution. At low incident energies, the expectation is that the CO projectile traps in the surface van der Waals well, undergoes many "memory destroying" collisional interactions, and then desorbs with its internal (rotational) and external (translational) degrees of freedom in equilibrium with the surface temperature ($T_{rot} \approx T_{trans} \approx T_S$). In our model, the scattering probability ($P_{scatter}$) is expressed as a product of an out-of-plane ($v_y = v_{Doppler}$) Maxwell–Boltzmann (MB) distribution times a thermalized rotational distribution

$$P_{scatter}(J, v_{Doppler}) = P_{MB}(v_{Doppler}, T_{trans})\, P_{rot}(J, T_{rot}) \quad (3)$$

which allows us to characterize independent transverse Doppler and rotational distributions by different temperatures ($T_{trans} \neq T_{rot}$). If these two temperatures are both experimentally indistinguishable from the surface temperature ($T_{trans} \approx T_{rot} \approx T_S$), detailed balance considerations[7] imply that the incident CO undergoes complete thermalization and desorbs without any barrier restricting the exit channel dynamics.

However, this is decidedly not what is observed, as evident in Figure 2A from a Boltzmann plot of the rotational-state populations for CO scattering from PFPE at room temperature. Instead, the CO rotational distributions exhibit thermal Boltzmann-like behavior but with a "temperature" (solid red line) that is significantly colder ($\Delta T \approx -45(3)$ K) than the surface (T_S = 293.1(1) K, blue dashed line). This absence of complete equilibration with the surface is further corroborated by high-resolution Doppler profile data in Figure 2B for which distinctly subthermal scattering "temperatures" are also noted in least squares Gaussian fits to the out-of-plane velocity distributions, with comparison of the model fit with sample data summarized in Figure 3. Also worth noting is that, although both the translational and rotational "temperatures" are clearly out of equilibrium with the liquid, they are indistinguishable from each other within experimental uncertainty ($T_{rot} \approx T_{trans} < T_S$). Thus, one simple physical picture for such behavior would be that the CO has enough interaction time with the liquid surface to equilibrate among its own internal/external (rotation/translation) degrees of freedom but still not enough time to equilibrate completely with the surface itself. It is important to note that the translational "temperature" data in these studies probe only velocity

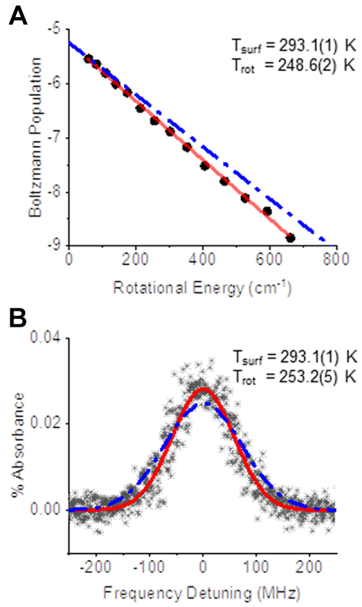

Figure 2. Sample data for CO scattering from room temperature squalane at E_{inc} = 1.0 kcal/mol. (A) Boltzmann plot of the rotational states. The blue dot-dash line represents a room-temperature rotational distribution, while the red solid line is the fit that predict subthermal behavior. Rotational populations for J = 5 through 18 are plotted. (B) Same as in (A) but for the translational degree of freedom for J = 8.

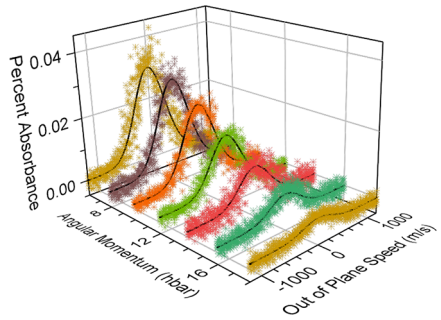

Figure 3. Sample least-squares fits (black line) to high-resolution CO(J) Doppler velocity profiles obtained from scattering of CO + squalane at room temperature. To avoid visual congestion, only the odd rotational states from J = 5–17 are shown out of the total J < 20 states detected.

https://dx.doi.org/10.1021/acs.jpcc.0c06400
J. Phys. Chem. C XXXX, XXX, XXX–XXX

components perpendicular to the scattering plane, with the corresponding *parallel velocity* components inaccessible to laser Dopplerimetry in the current experimental probe geometry.

We next explore the low-energy CO gas–liquid scattering dynamics as a function of both (i) the liquid and (ii) the liquid temperature, with results summarized in Figure 4. First of all,

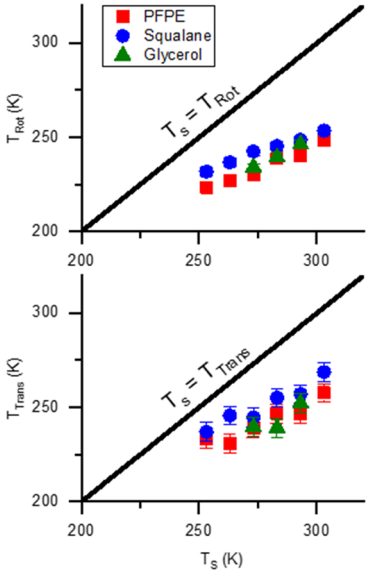

Figure 4. Temperature dependence of low-energy CO scattering for a series of liquids. The top panel shows the scattered rotational temperature (T_{rot}) as a function of T_S. The black line represents complete equilibration between rotational and surface temperatures. The bottom panel displays similar data and analysis with respect to the Doppler translational degree of freedom (T_{trans}). Error bars represent 1σ standard deviations of the mean. These measurements reflect population data obtained from J = 5–18 rotational states.

the data consistently indicate significant negative deviations ($\Delta T = T_{rot/trans} - T_S \approx -45(15)$ K) from full CO equilibration with the liquid surface, with both rotational and translational degrees of freedom indistinguishable and yet colder than T_S ($T_{trans} \approx T_{rot} < T_S$). Second, despite such deviations, there is nevertheless a clear sensitivity in the T_{rot} and T_{trans} values to the liquid temperature itself. Specifically, the $T_{trans} \approx T_{rot}$ values vary quasilinearly with changes in T_S, but with a subunity differential growth ($dT_{rot/trans}/dT_S \approx 0.50(8)$) over the range of experimentally accessible temperatures. Third, such deviations from full T_D equilibrium behavior are only weakly dependent on the nature of the liquid, with a greater equilibration toward T_S demonstrated for soft hydrophobic hydrocarbon (squalane) versus the more strongly interacting (glycerol or PFPE) gas–liquid interfaces. In summary, the rotational quantum state and Doppler-resolved experimental data provide evidence for *non-equilibrium scattering dynamics* at the gas–liquid interface, even at low collision energies ($E_{inc} \approx kT_S$) for which conventional wisdom would predict complete trapping desorption (TD) equilibrium behavior. To help provide physical insights into such non-equilibrium behavior, we turn next to molecular dynamics simulations in section IV, specifically attempting to model low-energy experimental scattering behavior for three projectiles (CO, DCl, and CO_2) at a perfluorinated, hydrophobic, and hydrophilic gas–liquid interface.

IV. MOLECULAR DYNAMICS SIMULATIONS

To probe the nature of "TD" equilibration (or lack thereof) with the surface, three different molecular projectiles have been explored: CO_2, CO, and DCl/HCl. Experimentally, all three molecules have been extensively characterized in gas–liquid scattering studies at low collision energies. As mentioned in the introduction, CO_2 and DCl/HCl thermalize with the gas–liquid surface at low E_{inc} while the present results clearly demonstrates that CO does not. By comparing the trajectory results from these three projectiles, a mechanism for why CO (vs DCl/HCl, CO_2) does not equilibrate and thermally desorb from the surface can be developed. To these ends, two series of molecular dynamics studies have been explored. The first series focuses on the temperature dependence (T_S) of CO surface scattering, which provides access to a much wider range of temperatures as well as permits direct comparison to experimental data. A second series looks at differences in scattering dynamics between the three probe molecules (nonpolar (CO) vs strongly dipolar (DCl) vs quadrupolar CO_2 projectiles) with scattering from a model perfluorinated liquid interface.

VI.A. CO, DCl, and CO_2 + FSAMs Potential Energy Surface. Molecular dynamics calculations from our group in collaboration with the Hase group have been previously described.[38] In the interest of simplicity, we direct these efforts first toward scattering of molecules from a perfluorinated interface, building on previous successes for theoretical modeling of quantum-state-resolved scattering. The simulated surface is a fluorinated self-assembled monolayer (FSAM), which has been shown to be an accurate yet computationally feasible proxy for the liquid, PFPE.[39,40] As implemented previously, a sample surface is constructed from 48 fluorinated thiol radicals, $CF_3(CF_2)_7S$, chemisorbed onto a slab of Au(111) by a harmonic Au–S stretch potential. This slab of gold atoms is fixed in space and used to define the surface and its unit cell. Motions for the other atoms in the chain are governed by additional potentials that involve two-atom stretches, three-atom bends, and four-atom torsions. Atoms in the chains interact with each other through atom–atom nonbonding potentials that are constructed from the sum of an exponential repulsion and C/r^n attraction term, with published parameters for each of these expressions.[38]

The CO_2-PFPE potential energy surface (PES) has been generated by Hase and co-workers and utilized extensively by Perkins et al. New surfaces for the CO and H/DCl gas-SAM potentials have been developed for the present study according to the same principles. Briefly, *ab initio* radial 1D scans have been calculated for both CO and HCl approaching CF_4 from a series of Euler approach (ϕ, θ, χ) angles, with the CF_4 molecule serving as proxy for a CF head group at the gas-polyfluorinated liquid (PFPE) interface. For each intermolecular geometry, high-level *ab initio* calculations are performed with explicitly correlated (f12) electron methods at the CCSD(T)-f12 level of theory (MOLPRO software platform)[41] with f12 correlation consistent Dunning basis sets (AVnZ-f12; n = 2,3,4), counterpoise correction for basis set superposition error (BSSE), and extrapolation to the complete basis set limit (CBS).[42–47] This set of *ab initio* energy values is then fit to a two-body atom–atom expression utilizing Lennard–Jones type exponential repulsion/inverse power law attraction/repulsion terms

https://dx.doi.org/10.1021/acs.jpcc.0c06400
J. Phys. Chem. C XXXX, XXX, XXX–XXX

$$V_j(r_j) = \sum_i A_i e^{-k_i r_j} + \sum_i B_i r_j^{-n_i}$$

where r_j is the two-body spacing for the j^{th} pair of atoms. Such a PES construction protocol has been used in the generation of the corresponding potential for CO_2-FSAMs scattering dynamics, which demonstrates remarkably quantitative agreement with experiment.[40]

We note that such gas-SAMs PES data have distinct repulsive/attractive regions on very different energy/length scales. Thus, any nonweighted least-square fit over a uniform grid spacing will yield results sensitive to the *ad hoc* choice of the grid range sampled, typically oversampling the repulsive hard wall (high E) and underweighting both the van der Waals well region and long-range attractive parts (low E) of the potential. This is especially relevant for scattering at low incident energies for which the trajectories do not sample high up on the repulsive wall. To counterbalance these effects, we implement a weighted least-square fit which more democratically samples the three dynamically relevant regions (repulsive wall, van der Waals well, and attractive long range) of the potential. The empirical weighting function used is of the form

$$W(E_{inc}) = (E_{inc} + E_{off})^{-2}$$

with the offset energy ($E_{off} > 0$) chosen to prevent divergence at low E_{inc} and regulate how quickly the weights decrease with increasing energy. For a given CF_4–molecular projectile combination, E_{off} is chosen empirically such that the weight at the bottom of the van der Waals well is approximately 16-fold larger than at $E_{inc} = 0$. By way of example, Figure 5

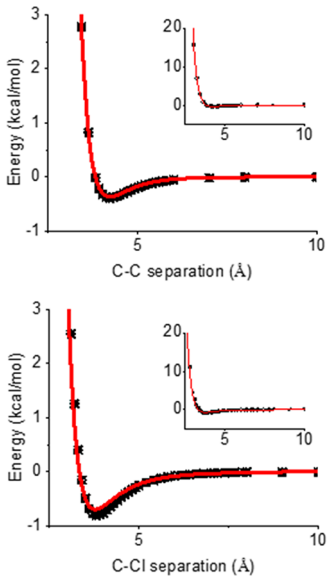

Figure 5. Sample *ab initio* CCSD(T)-f12/AVnZ (n = 2,3,4 CBS) potential slices for OC–CF_4 (C–C distance, top) and DCl–CF_4 (C–Cl distance, bottom), with the analytic least-squares atom-atom fit to the full potential energy surface (PES) shown in red. See text for details. The insets show the PES over a larger energy scale.

displays sample cuts of the calculated and least-square-fitted PES for both CF_4-CO and CF_4-H/DCl potentials at $E_{inc} < 3$ kcal, as well as insets showing this good agreement extending to higher incident energies. The optimized least-square-fitted coefficients (A_i, k_i, B_i, n_i) for both CO-CF_4 and H/DCl-CF_4 potential energy surfaces are summarized in Tables 1 and 2. Within the context of the Born–Oppenheimer approximation, the potentials are identical for both CF_4-HCl and CF_4-DCl.

Calculations for the CO_2–CF_4 van der Waals complex have been discussed in great detail by Hase and co-workers.[38] The lowest energy configuration for this complex is C_{2v} symmetry with the carbon from the CO_2 approaching between two of the fluorine's with a carbon–carbon distance of 3.76 Å and a well depth of −0.82 kcal/mol. For H/DCl-CF_4, the lowest energy geometry is of low symmetry (C_s) and not significantly sampled in the random trajectories calculated. The lowest energy configuration calculated is with the chlorine centered between three of the CF_4's fluorines with the hydrogen pointing perpendicular to this axis eclipsing the fluorine when looking down the symmetry axis, with a carbon–chlorine distance of 3.8 Å and a depth of −0.83 kcals/mol. Naively, we thought that the bound state would be of C_{3v} symmetry with the hydrogen pointing toward the central carbon, but due to the large polarizability of the chlorine and the large size of the fluorines, the hydrogen is pushed out of the way leading to a bound state of the C_s symmetry. The final projectile, CO, is quite interesting since it has two near identical wells. The lower energy configuration is where the carbon of the CO is facing the carbon of the CF_4 with a carbon–carbon distance of 3.65 Å and a well depth of −0.667 kcals/mol. The other bound well is with the oxygen of the CO facing the CF_4's central carbon. This has a carbon–carbon distance of 4.55 Å (with a carbon–oxygen distance of 3.42 Å) and a well depth of −0.665 kcals/mol.

VI.B. Trajectories: Low-Energy Collisions of CO, DCl, and CO_2 with FSAMs. Scattering trajectories are calculated using the package VENUS05 developed by Hase and co-workers,[48] propagated with sufficiently small timesteps ($\Delta t \approx 0.2$ fs) to ensure energy conservation ($\Delta E/E < 50 \times 10^{-9}$) over the time scale of a typical 10,000 fs trajectory. To permit temperature control of the gas–liquid interface, each trajectory is initiated with FSAM momenta sampled from a Boltzmann distribution at T_S. The FSAM simulation is then propagated for 2000 fs, with the atomic velocities uniformly rescaled after every 100 fs to equilibrate the atom ensemble to a well-defined temperature and average kinetic energy (i.e., $\langle E \rangle = 3/2kT_S$). The CO, DCl, and CO_2 projectiles are prepared asymptotically ($z_{init} = 30$ Å from the surface) in an initial state corresponding to uniform 2D angular sampling of the molecular orientation and zero rotational energy ($J = 0$). The total incident linear momentum of the projectile is kept constant from trajectory to trajectory, with the first point of contact randomized by 2D translation over an area equivalent to a single FSAM unit cell. The trajectory is then propagated such that the projectile collides with and rebounds sufficiently far from the surface for any residual projectile-surface interaction to be negligible, either by final height ($z_{final} > z_{init} = 30$ Å) or total time interval ($T_{final} > 100{,}000$ fs). The final projectile velocity components and kinetic energies are taken directly from the last simulation point for which the angular momentum J is sorted into bins of $\hbar$ width from the final simulation value of $\langle J^2 \rangle \approx J(J+1)\,\hbar^2$.

VI.C. Theoretical Results and Analysis: CO with FSAMs. We are now in a position to analyze the molecular dynamics (MD) trajectories on the same footing as the original quantum-state-resolved experimental data. The first and simplest comparison to make is between experimental and theoretical "temperatures" for low-energy ($E_{inc} = 1.0(1)$ kcal/mol) scattering of CO molecules from liquid PFPE (experiment, Figure 4, red symbols) and FSAMs (MD simulation,

https://dx.doi.org/10.1021/acs.jpcc.0c06400
J. Phys. Chem. C XXXX, XXX, XXX–XXX

Table 1. Least-Squares-Fitted Parameters for the CO-FSAMs Atom−Atom Potential, as Obtained from Least-Squares Fits to High-Level *Ab Initio* CCSD(T)-f12/AVnZ-f12 (n = 2,3,4,CBS) Calculations for a Systematic Series of CO Approaches to CF_4. See Text for Details

CO	A (Kcal/mol)	K ($Å^{-1}$)	B_1 (Kcal/mol × $Å^n$)	n_1	B_2 (Kcal/mol × $Å^n$)	n_2
C−C	N/A	N/A	−0.0003	6.439181	0.000295	12
C−F	38041.37	3.488949	−2589.46	7.180264	2589.459	12
O−C	N/A	N/A	−11435.6	9.405355	11435.55	12
O−F	141,479	4.218949	−7845.65	8,822,076	7845.652	12

Table 2. Least-Squares-Fitted Parameters for the HCl-FSAMs Atom−Atom Potential, as Obtained from Least-Squares Fits to High-Level *Ab Initio* CCSD(T)-f12/AVnZ-f12 (n = 2,3,4,CBS) Basis Set Superposition Error (BSSE)-Corrected Calculations for a Systematic Series of HCl Approaches to CF_4. See Text for Details

HCl	A (Kcal/mol)	K ($Å^{-1}$)	B (Kcal/mol × $Å^n$)	n
Cl−C	516798.9	3.722796	−397405	10.44609
Cl−F	75540.76	3.888306	−318.235	5.637447
H−C	6261.853	2.979897	−229.865	4.963686
H−F	266.2704	3.55146	N/A	N/A

Figure 6, black symbols). To extract a temperature (T_{rot}) from the rotational degree of freedom, we least-square fit the final

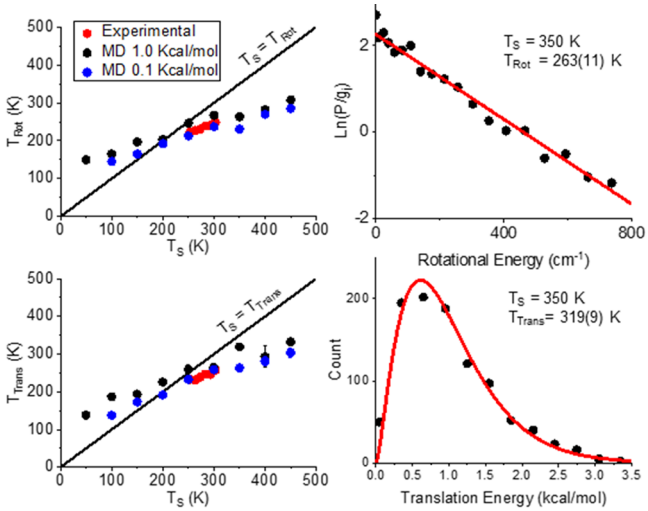

Figure 6. Comparison of MD and experimental temperature dependence. The left panels show the rotational (top) and translational (bottom) temperature dependence. The right panels show example fits to the MD data at a surface temperature of 350 K. Black and blue points reflect simulated data; the red data points are experimental.

CO(J) states to a single-temperature Boltzmann distribution, a sample log plot of which for CO scattering from FSAMs is reported (T_S = 350 K) in the upper right panel of Figure 6. Noteworthy is the remarkable agreement between the experimental T_{rot} values extracted from CO scattering data (as summarized in Figure 4) with the theoretical T_{rot} values in Figure 6A obtained from analysis of the low-energy MD trajectory data, although now accessible over a much broader dynamic range (T_S ≈ 50−450 K vs T_S ≈ 275-325 K). Also worth noting is that such good agreement between experiment and theory is largely insensitive to incident energy, with MD trajectory data at an order of magnitude lower E_{inc} ≈ 0.1 kcal/mol yielding only slightly cooler (blue symbols, Figure 6A) but essentially indistinguishable results from the E_{inc} ≈ 1.0(1) kcal/mol scattering data (black symbols, Figure 6A). Furthermore, the theoretical T_{rot} data exhibit the same *quasilinear incremental* dependence on FSAM temperature. Specifically, differential slopes ($m \approx dT_{rot}/dT_S \approx 0.42(3)$) from the MD simulations are in reasonable agreement with the values ($m \approx dT_{rot}/dT_S \approx 0.49(5)$) determined experimentally for CO + PFPE (see Figure 4). Simply summarized, the CO(J) distributions for low-energy collisions (E_{inc} ≈ 1.0 kcal/mol) at the gas−PFPE liquid interface scatter with a rotational temperature colder than ($\Delta T \approx -53$ K at T_S = 300 K) and differential slopes ($m \approx 0.49(5)$) indicating sensitivity to the surface temperature (T_S). These trends are in close agreement with theoretical trajectory data for CO + FSAMs over a much wider temperature window (see Figure 6A) than is experimentally accessible in the liquid phase.

In a similar fashion, we next analyze the trajectory calculations for translational distributions in the scattered CO flux at low incident energies. We find that fits to a normal flux weighted probability distribution ($F(v_x,v_y, v_z) \propto v_z \exp(-m(v_x^2 + v_y^2 + v_z^2)/2kT_{trans})$ and temperature (T_{trans}) already yield satisfactory agreement with the data. We thus report global fits to a single-translational temperature (Figure 6, lower left panel), which yield statistics with low scatter for the full set of N = 1000 trajectories (see Figure 6B right panel for a sample speed distribution) than each degree of the freedom fit independently. The MD scattering data for CO + FSAMs again yield translational temperatures varying linearly with T_S and in remarkably good agreement with the experimental CO + PFPE results. Analysis of the translational data provides additional experimental/theoretical support for CO scattering from a FSAMs surface in a temperature distribution that is both (i) colder than ($\Delta T \approx -45(15)$K) and (ii) differentially proportional to ($dT_{trans}/dT_S \approx m \approx 0.50(8)$) the liquid temperature over our experimentally accessible window of observation. The combined experimental and theoretical results for CO are in fundamental disagreement with a conventional picture of 100% trapping desorption (TD) dynamics dominating at low collision energies, which in the absence of transition state barrier would predict complete equilibration ($T_{rot} \approx T_{trans} \approx T_S$) with the liquid surface temperature at all values of T_S.

The trajectory data obtained over this more expanded temperature range in Figure 5 reveal additional insights into the scattering dynamics. Specifically, the theoretical plots for $E_{inc} \approx 1.0(1)$ kcal/mol intersect the $T = T_S$ line and are therefore predicted to cross from a regime of subthermal scattering ($T < T_S$) at near room temperatures into a nominally "hyperthermal" scattering regime ($T > T_S$) at sufficiently low surface temperatures. Indeed, this stimulated a parallel set of trajectory studies at 10-fold lower collision energies (E_{inc} = 0.1 kcal/mol, see Figure 5), which clearly reiterate the same subthermal to hyperthermal crossover near

https://dx.doi.org/10.1021/acs.jpcc.0c06400
J. Phys. Chem. C XXXX, XXX, XXX−XXX

$T_S \approx 200$ K. This nonphysical result is inconsistent with full TD equilibrium predictions for which one would expect T_{rot}, T_{trans} to asymptotically approach but never cross T_S. This provides first unambiguous evidence that the energy transfer dynamics are still far from the TD scattering regime even down at E_{inc} = 0.1−1.0 kcal/mol. Instead, with CO−FSAMs well depths of ≈ 0.5 kcal/mol, these collision dynamics sample an incident energy window competitive with long-range interactions between the projectile and liquid surface atoms. As a final note, even lower temperature MD simulations (E_{inc} = 0.1 kcal/mol and T_s = 50 K) were also attempted; however, none of these trajectories resulted in successful desorption of the CO from the FSAMs surface within the 100 ps observation window. By way of one simple interpretation, this would be consistent with a sticking coefficient for CO that reaches unity at sufficiently low surface temperatures and collision energies.

VI.D. Theoretical Results and Analysis: DCl and CO_2 with FSAMs. Although the MD results empirically match experimental observations quite well, they do not yet provide an answer why CO molecules desorb from the surface at temperatures below T_S. To achieve a further insight, we have extended these MD simulations to all three projectiles (CO, DCl, and CO_2) colliding with a FSAM model surface, each of which have been experimentally studied with PFPE liquid in quantum-state-resolved experiments. These three molecules are quite different in terms of their interactions with surface CF bonds, corresponding to van der Waals dipole-induced dipole (CO-CF), dipole−dipole (D/HCl-CF)[49] versus dipole−quadrupole (OCO-CF).[50] Since DCl and CO_2 have been shown to experimentally equilibrate with PFPE at low collision energies, we thus anticipate nearly full thermalization in the MD simulations to $T_S \approx 300$ K.

The final quantum-state populations from these additional molecular trajectories are analyzed in identical fashion to the previous CO + FSAM data in section IV.B, with T_S = 300 K. As expected, CO_2 and DCl do scatter from FSAM with near thermal rotational temperatures, specifically $T_{rot} \approx 305(10)$ K and $T_{rot} \approx 287(12)$ K, respectively. Similarly, we also observe fully equilibrated results in the DCl and CO_2 translational degrees of freedom, with temperatures from least-square fits to out-of-plane velocity profiles of T_{trans}(DCl) = 309(7) K and T_{trans} (CO_2) =304(7) K. This is in clear contrast with the CO trajectory behavior, which consistently scatters from an FSAM interface (T_S = 300) with subthermal rotational (T_{rot} = 266(9) K) and translational (T_{trans} = 264(6) K) temperatures. In summary, the MD theoretical predictions for each of these three projectile + gas−liquid interfacial trajectory simulations match closely what has been experimentally observed from actual quantum-state-resolved scattering studies.

VI.E. Interaction Time Analysis: CO, DCl, CO_2 with FSAMs. The excellent agreement between MD simulations and experimental results motivates a deeper statistical analysis into the trajectories themselves. One crucial observable is the interaction time (τ) of the molecule on the surface, which can be determined from durations over which the gas-surface forces exceed some threshold. This threshold is chosen to be 10× the root-mean-square force magnitude (f_{RMS}) over the first 3 ps of the simulation, during which the molecule is 30 Å away from and does not interact appreciably with the surface. This provides time for an estimate of a force "noise floor" due to machine precision, which permits establishing a threshold distance for detectable interaction of the projectile with the surface. The level chosen is roughly 10 times higher than machine precision, sufficiently low that every trajectory crosses this level only twice, once when it starts to interact with the surface and once when it leaves the surface. If the desorption was a 1st order kinetic process, we would expect the gas−liquid collisional durations to be exponentially distributed, with a slope reflecting the lifetime of the molecule−surface complex. The threshold level above is ∼10 Å above the surface, and thus, there will be small additional contributions to this extracted value from the flight time of the leaving molecules. However, this spread is only ∼1−3 ps on average and thus has negligible impact on the extracted molecule surface complex lifetimes.

Semilinear plots of the corresponding exponential decays are exhibited in Figure 7, along with linear least-square fits to extract the corresponding projectile-surface residence lifetimes. As expected, the residence times on this surface are indeed well characterized by single exponential decay, with lifetimes on the 10−30 ps range. Interestingly, there is a clear 2−3-fold increase in surface residence lifetimes for the more strongly (τ_{CO2} = 28(1) ps and τ_{DCl} = 19(1) ps) versus less strongly (τ_{CO} = 9(1) ps) interacting projectiles. Only a very small fraction of events is observed with lifetimes in excess of the maximum cutoff trajectory duration (T_{cutoff} = 100 ps), specifically, 0, 1, and 5% for CO, DCl, and CO_2 respectively. As expected, this is in the same order as the 1/e lifetimes of collisional durations and in reverse order with respect to potential well depths for the gas−liquid binding interactions (see Figure 5). Similarly, instead of looking at the length of time the molecule interacts with the surface, we can look at the number of classical turning points the molecule undergoes during its trajectory. This reports on the frequency of reversals (i.e., turning points) in the normal center of mass momentum and can be seen to be approximately twice the number of times the molecule attempts to leave the surface. For the three scatterers, we see a similar trend to the surface residence times. CO undergoes an average of ∼6 classical turning points, meaning that it requires on average of only three attempts to leave the surface before it successfully desorbs. This is in clear contrast to the two other projectiles, with DCl undergoing ∼19 classical turning points and CO_2 undergoing ∼35. In summary, it requires 6−10-fold fewer attempts for CO to desorb from the FSAM surface than for the other two molecules.

An even more insightful metric can be obtained from the distribution of gas−liquid surface heights $P(z)$ over a full time dependent scattering trajectory. This is extracted by sampling the center of mass for each projectile (CO, DCl, CO_2) every 2

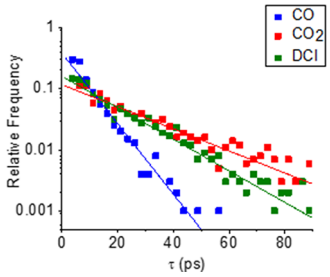

Figure 7. Histograms of surface FSAM interaction times in MD simulations for low-energy scattering with each of the three projectiles. The fractions of trajectories that do not result in escape from the surface after 100 ps trajectories for CO_2, DCl, and CO are 5, 1, and 0%, respectively.

https://dx.doi.org/10.1021/acs.jpcc.0c06400
J. Phys. Chem. C XXXX, XXX, XXX−XXX

fs (10 time steps) and recording the height (z) above the gas−liquid interface. The three sets of data from all N = 1000 trajectories are then histogrammed (Δz = 0.1 Å bins), normalized to unit incident flux, and displayed on the same scale in Figure 8. The surface height (z = 0) was determined by

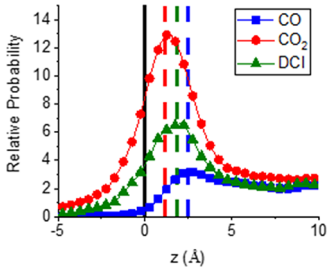

Figure 8. The probability distribution of the three molecules probed as a function of height above the surface. The dotted lines show each of the peaks of the distributions in relation to the surface height at z = 0 (black line).

looking at the distribution of the surface fluorines and finding their time averaged 50% density position above the Au surface, which provides a suitable reference point for referencing the whole surface. The resulting plots exhibit a qualitatively similar topology for each projectile, with (i) a flat asymptotic approach probability (z > 5 Å), (ii) strong peaking in the adsorption well region (0 Å < z < 5 Å), and (iii) rapid probability decay as the projectile penetrates into the FSAM surface. However, there are also important differences between the plots for CO versus DCl/CO_2 projectiles, which in turn inform critical differences in the collision dynamics. For example, CO exhibits a much weaker statistical presence in the well region, with a maximum relative probability density (P_{well} ~1.7) 2−3-fold smaller than for DCl (P_{well} ~3.3) or CO_2 (P_{well} ~5.5). As expected for a 1st order exponential process, these values are in excellent agreement with ratios of observed residence lifetimes (see Figure 7). Furthermore, if we look more closely at the well region, the CO probability density peaks at z_{max} ~2.50(10) Å from the surface while the maxima for DCl and CO_2 occur at ~2.00(10) and ~1.25(10) Å respectively. Simply summarized, histogram analysis of the trajectories indicates that CO is (i) trapped substantially more shallowly than DCl or CO_2 and (ii) spends more of its residence time further away from the FSAMs surface.

Finally, an even subtler but more quantitative tool with which to represent such statistical data is the potential of mean force (POMF), represented by

$$V_{POMF}(z) = -kT_B \ln[P(z)]$$

Under equilibrium conditions, V_{POMF} characterizes the relative probability for a projectile a distance z above the gas−liquid interface in terms of a distance-dependent free energy, i.e., $\Delta G(z) \sim V_{POMF}(z)$. However, it provides an equally meaningful probability distribution *under* non-equilibrium conditions, as obtained from calculations of the force normal to the surface for each of the bin heights and integrating the reversible work from infinity back to the gas−liquid interface. The values of this *non-equilibrium potential of mean force* ($V_{POMF}(z)$) have been calculated from the trajectories (Figure 8) and are plotted in Figure 9. As noted previously for the surface height distributions (Figure 8), there are three characteristic domains labelled as (i) asymptotic, (ii)

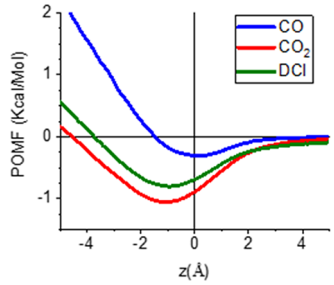

Figure 9. Calculated potentials of mean force, $V_{POMF}(z)$, for CO, CO_2, and DCl projectiles with respect to distance from the FSAM surface.

van der Waals well, and (iii) repulsive wall regions, where we have chosen z = 0 as the point at which the average fluorine density has decayed to 50% of its bulk value. Of particular importance, both CO_2 and DCl projectiles exhibit minima penetrating into the liquid (z < 0), whereas the well for CO is more nearly centered on the gas−liquid interface itself. Profound differences can be seen in the V_{POMF} well depths for these three projectiles, with the CO POMF well depth (0.3 kcal/mol) 3−4 times shallower than either DCl (0.8 kcal/mol) or CO_2 (1.1 kcal/mol). Additionally, V_{POMF} for CO in the repulsive region (left side of Figure 9) increases with a slope of $m \approx 0.6$ kcal/mol/Å, while both CO_2 and DCl exhibit notably shallower slopes of $m \approx 0.4$ kcal/mol/Å. In summary, CO + PFPE thus clearly exhibits (i) a weaker attractive well, (ii) a $V_{POMF}(z)$ minimum shifted notably outward, and (iii) more steeply repulsive interactions with the surface than experienced by either DCl or CO_2 projectiles, respectively.

V. DISCUSSION

The combined experimental and theoretical results in this paper reveal anomalous behavior for supersonically cooled CO(J = 0) scattering at low energies ($E_{inc} \approx 0.1-1.0$ kcal/mol) from the gas−liquid interface, specifically CO desorbing at rotational and translational temperatures (i) out of equilibrium with and (ii) colder than the surface (T_S). This is fundamentally at odds with conventional detailed balance considerations for which trapping desorption (TD) events might be expected to dominate in the limit of low collision energies and unity sticking coefficients (α = 1). A simple mechano-kinetic view of the TD process is summarized by three stages. (1) The projectile approaches the surface at sufficiently low energy for all incoming molecular states to become transiently bound in a physisorption well. (2) The molecule undergoes extended collisional interactions with the surface sufficient to thermalize with the liquid (T_S) and lose all residual memory of the incident collision. (3) The thermalized molecule eventually leaves the surface through a barrierless exit channel, which by detailed balance requires the asymptotic scattering-state distributions to be accurately described by the surface liquid temperature, T_S. Experimental evidence in this work argues that CO does not leave the surface at T_S and thus clearly diverges from this putative TD pathway. The question of interest is where?

A first place to look would be the final desorption from the liquid interface for which the crucial assumption is that a molecule leaves along a monotonic and barrierless pathway. From atom−atom modeling of the gas−liquid potential, this assumption seems secure: the potential energy surface for all three projectiles rises monotonically from the bound well to

https://dx.doi.org/10.1021/acs.jpcc.0c06400
J. Phys. Chem. C XXXX, XXX, XXX−XXX

infinite separation. This is true not only for the static atom−atom PES but also for the thermodynamically averaged potential of mean force (POMF). We can therefore be reasonably confident that the molecules do not experience transition-state barriers and thus complex desorption dynamics (step 3) cannot explain why CO comes off the surface both translationally and rotationally colder than T_S.

We next consider the thermalization step 2 for which a TD event requires the projectile to undergo many interactions before leaving the surface. For a molecule trapped in a well and interacting with a thermal bath, the average residence time of the molecules should be described by Arrhenius behavior, with the first order rates decreasing (exponentially) with surface cooling. At sufficiently low temperatures, the slow rate constant for desorption is swamped by energy transfer to/from the surface, and thus, the projectile has ample time to thermalize. But with increasing T_S, the Arrhenius desorption rate increases more rapidly than the molecule-surface equilibration rate. For initially jet-cooled projectiles ($T_{rot} \approx 10$ K $< < T_S$) at low incident energies, as a result, one expects deviation in the desorption temperature below T_S (as observed), corresponding to a "roll off regime" as energy equilibration with the surface fails to compete with decreasing residence times. Experimentally, we see such suppression of equilibration dynamics (i.e., $T_{rot/trans} < T_S$) over the entire range of liquid temperatures accessible. Due to freezing points of the three (PFPE, squalane, and glycerol) liquids investigated, we are not able to reach lower temperatures experimentally, but the MD trajectory analysis empirically reveals that we are (i) already in this roll off regime for CO scattering under near room-temperature conditions and that these distributions become hyperthermal ($T_{rot} = T_{trans} > T_S$) at slightly lower temperatures. In summary, there is ample evidence in the MD simulations for nonthermalization and profound deviation from the TD dynamical paradigm. This is required for the scattered CO flux at low incident energies to exhibit a final translational/rotational quantum-state distribution temperature lower than T_S, as experimentally observed.

As a parting comment, we note that step 2 may not be the only weak link in violation of the TD scattering paradigm. We consider the initial trapping event (step 1), which for a true TD event would rigorously require CO to become trapped in the well long enough to lose all memory of the incident collision conditions. Looking back at the MD simulations in section IV, one could argue equally strongly that CO never "traps" on the surface long enough to lose complete memory. Indeed, the key difference we see between (nonthermalizing) CO and the (thermalizing) DCl/CO_2 projectiles is that CO spends a 2−3-fold shorter time in the vicinity of the surface, clearly uncharacteristic with trapping desorption (TD) but rather an impulsive scattering (IS) pathway. Although unconventional to think of low-energy inelastic gas−liquid scattering in this context, one simple physical interpretation could be that CO never interacts strongly enough with the liquid interface to either trap or equilibrate on the time scale of the collision event. Such novel collision dynamics might therefore best be characterized as a novel "subthermal impulsive scattering" (STIS) channel opening up at collision energies on the order of the well depth. Although further experimental and theoretical work will be required to support or refute such an interpretation, the existence of short-lived, impulsive scattering at low energies serves to highlight the greater dynamical richness of collision pathways than previously considered in the early TD/IS models for quantum-state-resolved scattering dynamics at the gas−liquid interface.

VI. SUMMARY AND CONCLUSIONS

Low energy scattering (E_{inc} = 1.0(1) kcal/mol) of CO has been studied from a systematic series of gas−liquid interfaces, exploiting high-resolution infrared absorption methods to probe the final translational (out to plane $v_{Doppler}$) and rotational (J) quantum-state distributions. The experimental studies reveal that CO scatters into a distribution characterized by distinctly *subthermal* (but nearly equivalent) rotational (T_{rot}) and Doppler translational (T_{trans}) temperatures ($T_{rot} \approx T_{trans} < T_S$). The results are fundamentally inconsistent with a traditional picture of complete accommodation (trapping-desorption, TD) at low incident energy of molecular scattering events from the gas−liquid surface.

To explore the physical origins of such phenomena, molecular dynamics simulations of CO, DCl, and CO_2 projectile scattering from a fluorinated self-assembled monolayer (FSAM) interface have been implemented, with atom−atom potentials modeled on high-level *ab initio* MOLPRO calculations (CCSD(T)-f12/AVnZ-f12 (n = 2,3,CBS)) as a function of CF_4−projectile distance/approach angle and corrected for basis set superposition error (BSSE). These potential energy surfaces have then been implanted in the framework of the Venus molecular dynamics program to probe energy transfer and accommodation dynamics over an expanded range of collision energies and liquid temperatures, revealing remarkably quantitative agreement with experimental results. Detailed statistical analysis of the molecular dynamics permits comparison between CO_2, DCl, and CO trajectories to elucidate mechanisms for projectile equilibration (or lack thereof) at the gas−liquid interface. Specifically, CO spends less time in the vicinity of the liquid interface and penetrate less deeply into the fluorinated surface compared to DCl and CO_2 projectiles. This difference in behavior has been statistically reiterated by potential of mean force ($V_{POMF}(z)$) calculations, which highlight a 2−3-fold *weaker well* depth and 2−3 times *steeper repulsive wall* for an CO-FSAM versus DCl-/CO_2-FSAMs potential energy surfaces. The experimental and theoretical quantum-state-resolved data reveal that CO does not trap long enough at low energies on the gas−liquid interface to result in complete energy equilibration with the liquid T_S. Instead, we argue that the experimental CO distributions violate the conventional paradigm of low-energy scattering through complete equilibration with the liquid and are indeed more consistent with a novel "subthermal impulsive scattering" (STIS) pathway rather than a trapping-desorption (TD) event. The data provide mounting evidence for a greater richness of collision pathways than considered in the early TD/IS models for quantum-state-resolved scattering dynamics at the gas−liquid interface.

AUTHOR INFORMATION

Corresponding Author

David J. Nesbitt − *JILA, National Institute of Standards and Technology, and University of Colorado, Boulder, Colorado 80309, United States; Department of Physics and Department of Chemistry, University of Colorado, Boulder, Colorado 80309, United States;* orcid.org/0000-0001-5365-1120; Email: djn@jila.colorado.edu

https://dx.doi.org/10.1021/acs.jpcc.0c06400
J. Phys. Chem. C XXXX, XXX, XXX−XXX

Author

Timothy A. Livingston Large − *JILA, National Institute of Standards and Technology, and University of Colorado, Boulder, Colorado 80309, United States; Department of Physics, University of Colorado, Boulder, Colorado 80309, United States*

Complete contact information is available at: https://pubs.acs.org/10.1021/acs.jpcc.0c06400

Notes

The authors declare no competing financial interest.

■ ACKNOWLEDGMENTS

Ongoing support for this work has been provided by the National Science Foundation under grant CHE-1665271 from the Chemical, Structure, Dynamics and Mechanisms-A Program, with ancillary support for initial apparatus construction from PHY-1734006 (Physics Frontier Center Program) and Air Force Office of Scientific Research (FA9550-15-1-0090). We would also like to acknowledge the late Prof. William Hase for his intellectual generosity in getting us started with Venus molecular dynamics calculations, advice in developing high-level *ab initio* potential surfaces, as well as his general enthusiasm and passion for gas−liquid scattering dynamics. His leadership, insight, patience, and perpetual smile will be sorely missed by all who knew him.

■ REFERENCES

(1) Perkins, B. G.; Häber, T.; Nesbitt, D. J. Quantum State-Resolved Energy Transfer Dynamics at Gas-Liquid Interfaces: IR Laser Studies of CO_2 Scattering from Perfluorinated Liquids. *J. Phys. Chem. B* **2005**, *109*, 16396−16405.

(2) Hurlbut, F. C.; Beck, D. E. *U.C. Eng. Proj. Report He-150-166*; 1959.

(3) Cohen, S. R.; Naaman, R.; Balint-Kurti, G. G. Energy-Distribution between Spin-Orbit States in NO Scattered from Organized Amphiphilic Monolayers. *Chem. Phys. Lett.* **1988**, *152*, 269−273.

(4) Cohen, S. R.; Naaman, R.; Balint-Kurti, G. G. Investigation of NO Scattering from Organic Monolayers - Spin-Orbit State and Vibrational-State Population-Distributions. *Chem. Phys.* **1989**, *134*, 119−126.

(5) Perkins, B. G.; Nesbitt, D. J. Quantum-State-Resolved CO_2 Scattering Dynamics at the Gas-Liquid Interface: Incident Collision Energy and Liquid Dependence. *J. Phys. Chem. B* **2006**, *110*, 17126−17137.

(6) Saecker, M. E.; Nathanson, G. M. Collisions of Protic and Aprotic Gases with Hydrogen-Bonding and Hydrocarbon Liquids. *J. Chem. Phys.* **1993**, *99*, 7056−7075.

(7) Van Willigen, W. Angular Distribution of Hydrogen Molecules Desorbed from Metal Surfaces. *Phys. Lett. A* **1968**, *28*, 80−81.

(8) Tully, J. C. Dynamics of Gas-Surface Interactions: Thermal-Desorption of Ar and Xe from Platinum. *Surf. Sci.* **1981**, *111*, 461−478.

(9) Brown, L. S.; Sibener, S. J. A Molecular Beam Scattering Investigation of the Oxidation of CO on Rh(111). II. Angular and Velocity Distributions of the CO_2 Product. *J. Chem. Phys.* **1989**, *90*, 2807−2815.

(10) Hurst, J. E.; Becker, C. A.; Cowin, J. P.; Janda, K. C.; Wharton, L.; Auerbach, D. J. Observation of Direct Inelastic-Scattering in the Presence of Trapping-Desorption Scattering - Xe on Pt(111). *Phys. Rev. Lett.* **1979**, *43*, 1175−1177.

(11) Yan, T.; Hase, W. L. Origin of the Boltzmann Translational Energy Distribution in the Scattering of Hyperthermal Ne Atoms Off a Self-Assembled Monolayer. *Phys. Chem. Chem. Phys.* **2000**, *2*, 901−910.

(12) Perkins, B. G.; Nesbitt, D. J. Quantum-State-Resolved CO_2 Scattering Dynamics at the Gas-Liquid Interface: Dependence on Incident Angle. *J. Phys. Chem. A* **2007**, *111*, 7420−7430.

(13) Nathanson, G. M. Molecular Beam Studies of Gas-Liquid Interfaces. *Annu. Rev. Phys. Chem.* **2004**, *55*, 231−255.

(14) Wu, B.; Zhang, J.; Minton, T. K.; McKendrick, K. G.; Slattery, J. M.; Yockel, S.; Schatz, G. C. Scattering Dynamics of Hyperthermal Oxygen Atoms on Ionic Liquid Surfaces: [Emim][TNf_2] and [C_{12}mim][TNf_2]. *J. Phys. Chem. C* **2010**, *114*, 4015−4027.

(15) Tesa-Serrate, M. A.; Smoll, E. J., Jr.; Minton, T. K.; McKendrick, K. G. Atomic and Molecular Collisions at Liquid Surfaces. *Annu. Rev. Phys. Chem.* **2016**, *67*, 515−540.

(16) Tully, J. C. Washboard Model of Gas Surface Scattering. *J. Chem. Phys.* **1990**, *92*, 680−686.

(17) Zhang, J.; Upadhyaya, H. P.; Brunsvold, A. L.; Minton, T. K. Hyperthermal Reactions of O and O_2 with a Hydrocarbon Surface: Direct C-C Bond Breakage by O and H-Atom Abstraction by O_2. *J. Phys. Chem. B* **2006**, *110*, 12500−12511.

(18) Livingston Large, T. A.; Nesbitt, D. J. Quantum State and Doppler-Resolved Scattering of Thermal/Hyperthermal DCl at the Gas−Liquid Interface: Support for a Simple "Lever Arm" Model of the Energy-Transfer Dynamics. *J. Phys. Chem. C* **2019**, *123*, 3449−3460.

(19) Lednovich, S. L.; Fenn, J. B. Absolute Evaporation Rates for Some Polar and Nonpolar Liquids. *AIChE J.* **1977**, *23*, 454−459.

(20) Perkins; Nesbitt, D. J. Quantum State-Resolved CO_2 Collisions at the Gas-Liquid Interface: Surface Temperature-Dependent Scattering Dynamics. *J. Phys. Chem. B* **2008**, *112*, 507−519.

(21) Ringeisen, B. R.; Muenter, A. H.; Nathanson, G. M. Collisions of HCl, DCl, and HBr with Liquid Glycerol: Gas Uptake, D → H Exchange, and Solution Thermodynamics. *J. Phys. Chem. B* **2002**, *106*, 4988−4998.

(22) Ringeisen, B. R.; Muenter, A. H.; Nathanson, G. M. Collisions of DCl with Liquid Glycerol: Evidence for Rapid, near-Interfacial D → H Exchange and Desorption. *J. Phys. Chem. B* **2002**, *106*, 4999−5010.

(23) Chorny, I.; Benjamin, I.; Nathanson, G. M. Scattering, Trapping, and Ionization of HCl at the Surface of Liquid Glycerol. *J. Phys. Chem. B* **2004**, *108*, 995−1002.

(24) Hoffman, C. H.; Nesbitt, D. J. Quantum State Resolved 3D Velocity Map Imaging of Surface Scattered Molecules: Incident Energy Effects in HCl + Self-Assembled Monolayer Collisions. *J. Phys. Chem. C* **2016**, *120*, 16687−16698.

(25) Bagot, P. A. J.; Waring, C.; Costen, M. L.; McKendrick, K. G. Dynamics of Inelastic Scattering of OH Radicals from Reactive and Inert Liquid Surfaces. *J. Phys. Chem. C* **2008**, *112*, 10868−10877.

(26) Ziemkiewicz, M. P.; Zutz, A.; Nesbitt, D. J. Inelastic Scattering of Radicals at the Gas-Ionic Liquid Interface: Probing Surface Dynamics of Bmim-Cl, Bmim-BF_4, and Bmim-Tf_2n by Rovibronic Scattering of NO [$^2\Pi_{1/2}(0.5)$]. *J. Phys. Chem. C* **2012**, *116*, 14284−14294.

(27) Zutz, A.; Nesbitt, D. J. Nonadiabatic Spin-Orbit Excitation Dynamics in Quantum-State-Resolved NO($^2\Pi_{1/2}$) Scattering at the Gas-Room Temperature Ionic Liquid Interface. *J. Phys. Chem. C* **2015**, *119*, 8596−8607.

(28) Zutz, A.; Nesbitt, D. J. Quantum State-Resolved Molecular Scattering of NO ($^2\Pi_{1/2}$) at the Gas-[$C_n$mim][Tf_2n] Room Temperature Ionic Liquid Interface: Dependence on Alkyl Chain Length, Collision Energy, and Temperature. *AIP Adv.* **2016**, *6*, 105207.

(29) Kubiak, G. D.; Hurst, J. E., Jr.; Rennagel, H. G.; Mcclelland, G. M.; Zare, R. N. Direct Inelastic Scattering of Nitric Oxide from Clean Ag(111): Rotational and Fine Structure Distributions. *J. Chem. Phys.* **1983**, *79*, 5163−5178.

(30) Cavanagh, R. R.; King, D. S. Rotational- and Spin-State Distributions: NO Thermally Desorbed from Ru(001). *Phys. Rev. Lett.* **1981**, *47*, 1829−1832.

(31) McClelland, G. M.; Kubiak, G. D.; Rennagel, H. G.; Zare, R. N. Determination of Internal-State Distributions of Surface Scattered

Molecules - Incomplete Rotational Accommodation of NO on Ag(111). *Phys. Rev. Lett.* **1981**, *46*, 831−834.
(32) Hepburn, J. W.; Northrup, F. J.; Ogram, G. L.; Polanyi, J. C.; Willamson, J. M. Rotationally Inelastic Scattering from Surfaces CO(g) + LiF(001). *Chem. Phys. Lett.* **1982**, *85*, 127−130.
(33) Gisler, A. W.; Nesbitt, D. J. On Probing Ions at the Gas-Liquid Interface by Quantum State-Resolved Molecular Beam Scattering: The Curious Incident of the Cation in the Night Time. *Faraday Discuss.* **2012**, *157*, 297−305.
(34) Oh-e, M.; Yokoyama, H.; Baldelli, S. Structure of the Glycerol Liquid/Vapor Interface Studied by Sum-Frequency Vibrational Spectroscopy. *Appl. Phys. Lett.* **2004**, *84*, 4965−4967.
(35) Proch, D.; Trickl, T. A High-Intensity Multi-Purpose Piezoelectric Pulsed Molecular Beam Source. *Rev. Sci. Instrum.* **1989**, *60*, 713−716.
(36) Nizkorodov, S. A.; Harper, W. W.; Chapman, W. B.; Blackmon, B. W.; Nesbitt, D. J. Energy-Dependent Cross Sections and Nonadiabatic Reaction Dynamics in $F(^2P_{3/2}, {}^2P_{1/2})+nH_2 \rightarrow HF-(v,J)+H$. *J. Chem. Phys.* **1999**, *111*, 8404−8416.
(37) Weida, M. J.; Caffey, D.; Rowlette, J. A.; Arnone, D. F.; Day, T. Utilizing Broad Gain Bandwidth in Quantum Cascade Devices. *Opt. Eng.* **2010**, *49*, 111120.
(38) Martínez-Núñez, E.; Rahaman, A.; Hase, W. L. Chemical Dynamics Simulations of CO_2 Scattering Off a Fluorinated Self-Assembled Monolayer Surface. *J. Phys. Chem. C* **2007**, *111*, 354−364.
(39) Perkins, B. G., Jr.; Nesbitt, D. J. Toward Three-Dimensional Quantum State-Resolved Collision Dynamics at the Gas-Liquid Interface: Theoretical Investigation of Incident Angle. *J. Phys. Chem. A* **2009**, *113*, 4613−4625.
(40) Nogueira, J. J.; Vázquez, S. A.; Mazyar, O. A.; Hase, W. L.; Perkins, B. G., Jr.; Nesbitt, D. J.; Martínez-Núñez, E. Dynamics of CO_2 Scattering Off a Perfluorinated Self-Assembled Monolayer. Influence of the Incident Collision Energy, Mass Effects, and Use of Different Surface Models. *J. Phys. Chem. A* **2009**, *113*, 3850−3865.
(41) Werner, H.-J.; Knowles, P. J.; Lindh, R.; Manby, F. R.; Schütz, M.; Celani, P.; Korona, T.; Mitrushenkov, A.; Rauhut, G.; Adler, T. B.; Amos, R. D.; Bernhardsson, A.; Berning, A.; Cooper, D. L.; Deegan, M. J. O.; Dobbyn, A. J.; Eckert, F.; Goll, E.; Hampel, C.; Hetzer, G.; Hrenar, T.; Knizia, G.; Köppl, C.; Liu, Y.; Lloyd, A. W.; Mata, R. A.; May, A. J.; McNicholas, S. J.; Meyer, W.; Mura, M. E.; Nicklaß, A.; Palmieri, P.; Pflüger, K.; Pitzer, R.; Reiher, M.; Schumann, U.; Stoll, H.; Stone, A. J.; Tarroni, R.; Thorsteinsson, T.; Wang, M.; Wolf, A. *Molpro, Version 2009.1, a Package of Ab Initio Programs*; See http://www.Molpro.Net, 2009.
(42) Peterson, K. A. *Correlation Consistent Basis Sets*; Peterson Group Website: http://tyr0.chem.wsu.edu/~kipeters/basis.html, 2019.
(43) Hill, J. G.; Peterson, K. A.; Knizia, G.; Werner, H. J. Extrapolating MP2 and CCSD Explicitly Correlated Correlation Energies to the Complete Basis Set Limit with First and Second Row Correlation Consistent Basis Sets. *J. Chem. Phys.* **2009**, *131*, 194105.
(44) Van Duijneveldt, F. B.; Van Duijneveldt-van de Rijdt, J. G. C. M.; Van Lenthe, J. H. State of the Art in Counterpoise Theory. *Chem. Rev.* **1994**, *94*, 1873−1885.
(45) Chałasiński, G.; Szczęśniak, M. M. State of the Art and Challenges of the Ab Initio Theory of Intermolecular Interactions. *Chem. Rev.* **2000**, *100*, 4227−4252.
(46) Grimme, S. Accurate Description of Van Der Waals Complexes by Density Functional Theory Including Empirical Corrections. *J. Comput. Chem.* **2004**, *25*, 1463−1473.
(47) Peterson, K. A.; Dunning, T. H., Jr. Accurate Correlation Consistent Basis Sets for Molecular Core-Valence Correlation Effects: The Second Row Atoms Al-Ar, and the First Row Atoms B-Ne Revisited. *J. Chem. Phys.* **2002**, *117*, 10548−10560.
(48) Hase, W. L.; Duchovic, R. J.; Hu, X.; Komornicki, A.; Lim, K. F.; Lu, D.-h.; Peslherbe, G. H.; Swamy, K. N.; Vande Linde, S. R.; Varandas, A.; Wang, H.; Wolf, R. J. A General Chemical Dynamics Computer Program. *QCPE* **1996**, 671.
(49) Nelson, R. D., Jr.; Lide, D. R., Jr.; Maryott, A. A. *Selected Values of Electric Dipole Moments for Molecules in the Gas Phase*; National Standard Reference Data System: Washington, 1967.
(50) Graham, C.; Imrie, D. A.; Raab, R. E. Measurement of the Electric Quadrupole Moments of CO_2, CO, N_2, Cl_2 and BF_3. *Mol. Phys.* **1998**, *93*, 49−56.

https://dx.doi.org/10.1021/acs.jpcc.0c06400
J. Phys. Chem. C XXXX, XXX, XXX−XXX